Journal of Computational Physics 351 (2017) 108–120

Contents lists available at ScienceDirect

Journal of Computational Physics

www.elsevier.com/locate/jcp

A numerical method for predicting Rayleigh surface wave velocity in anisotropic crystals

Matthew R. Cherry [a,*], Shamachary Sathish [b], Ramana Grandhi [c]

[a] Air Force Research Labs, Materials and Manufacturing Directorate, 2230 10th St., WPAFB, OH 45433, USA
[b] University of Dayton Research Institute, Structural Integrity Division, Dayton, OH, USA
[c] Wright State University, Dayton, OH, USA

ARTICLE INFO

Article history:
Received 4 April 2017
Received in revised form 7 August 2017
Accepted 1 September 2017
Available online 5 September 2017

Keywords:
Rayleigh
Surface
Elastic
Velocity
Anisotropic

ABSTRACT

A numerical method was developed for calculating the Rayleigh Surface Wave (RSW) velocity in arbitrarily oriented single crystals in 360 degrees of propagation. This method relies on the results from modern analysis of RSW behavior with the Stroh formalism to restrict the domain in which to search for velocities by first calculating the limiting velocity. This extension of existing numerical methods also leads to a natural way of determining both the existence of the RSW as well as the possibility of encountering a pseudo-surface wave. Furthermore, the algorithm is applied to the calculation of elastic properties from measurement of the surface wave velocity in multiple different directions on a single crystal sample. The algorithm was tested with crystal symmetries and single crystal elastic moduli from literature. It was found to be very robust and efficient in calculating RSW velocity curves in all cases.

1. Introduction

Surface acoustic waves (SAW) such as Rayleigh surface waves (RSW) are important in a number of industries and applications such as nondestructive evaluation, materials characterization and acoustic microscopy. These waves propagate with distinct particle motions due to the mixing of both shear and compressional modes, and thus also have a different velocity. Furthermore, in an anisotropic material, the wave velocity and particle displacements change as a function of propagation direction. This is often represented with a slowness curve which gives the reciprocal of velocity as a function of propagation direction.

One application area for SAW's is in material property characterization. It has been shown in the past that measurement of RSW velocity on a single crystal in multiple directions of propagation can help calculate the single crystal elastic constants of a material [1]. More recently, modern experimental techniques have been used to measure the velocity of the surface waves much quicker than previously possible by relying on laser excitation and detection of elastic strains. In [2] the RSW velocity measurements were used to characterize the orientation map of a sample by calculating the velocity given known orientations and elastic constants and then inverting the response to get to orientation. In [3], the response over the entire surface of the sample was used to characterize the elastic properties of a material by generating a distribution of velocities in the many different orientations present in a polycrystalline aggregate. In all of these studies, a key step is accurately calculating the RSW velocity given known orientation, propagation direction, and elastic constants. These works all employed the methods of Farnell [4] for numerical computation of the RSW velocity.

* Corresponding author.
E-mail address: matthew.cherry.2@us.af.mil (M.R. Cherry).

http://dx.doi.org/10.1016/j.jcp.2017.09.002

While numerical methods have been used extensively in the past for calculation of the RSW velocity, there are a number of authors who have derived various equations for analytically calculating RSW velocities [5,6]. These derivations often rely on the Stroh formalism for elastodynamic equations, although not always [7]. This formalism reorganizes the stiffness matrix in an elastic wave problem and, after application of boundary conditions, results in an eigenvalue problem that combines the governing differential equation with the boundary condition to determine the wave propagation constant, ultimately leading to a polynomial equation whose roots are directly related to the wave velocity. With an application of rotation matrices to the elastic stiffness matrices, this problem could, in theory, be solved at any arbitrary orientation and propagation direction. However, the eigenvalue problem that results from the decomposition of the stiffness matrix is not analytically tractable in an arbitrarily rotated crystal also having arbitrary crystal symmetry. Even so, authors have used other methods and linear algebra techniques to argue past the eigenvalue problem and arrive at a new determinant equation for calculating the secular equation for RSW velocity explicitly [8]. This was done for an arbitrary elasticity tensor in [9], in which a determinant equation that was a function of only the elastic constants and wave velocity was used to derive various analytical secular equations that had previously been derived. Though this approach gives a very general method of calculating the coefficients of the secular equation explicitly as a function of elastic constants and rotation angles, the generalized version of the equations are very difficult to derive, even in symbolic math languages such as Mathematica. As a result, the equations are either solved for specific orientations, propagation directions, and crystal symmetries or numerical techniques are used to solve the equations [10].

While these analytical computations are not tractable for a generalized elasticity matrix, there are aspects of the derivation that can make the numerical solutions more stable and quicker. In this paper, a numerical technique for solving for the RSW velocity and pseudo-surface wave (PSW) velocity, as well as determining the existence of the RSW in an arbitrary direction on an arbitrarily oriented crystal is presented. The method is based on the typical iterative search procedure described in [4]. In that approach, the velocity space is searched over with non-gradient based optimization methods. In a situation in which the solver has found real eigenvalues (leading to non-decaying waves into the solid half-space, or non-surface wave behavior), the real eigenvalue that gives the lowest value of the boundary condition determinant is used. This leads to many different minima that become difficult to sort through in arbitrary cases. It also leads to discontinuous gradients of the boundary condition determinant with respect to velocity, preventing the use of gradient-based optimization routines. The typical approach to solving this problem is to perform the inverse many times and determine which minima corresponds to the RSW velocity. This results in a non-trivial solution time, so much so that the forward model is not used to directly compute the elastic constants, and a database approach is typically employed [2,11]. An alternate method for calculating the velocities is to perform simulations of the entire wave field using numerical simulations, e.g. [12–15]. These methods give a much more in depth view of the physics of the waves interacting with a complex anisotropic material and can be used to model the incident wave field, but they require significant computational resources relative to simply calculating the velocity using Farnell's method.

In the new numerical method described in the following sections, the limiting velocity is first found using an iterative search procedure. This provides a solid lower and upper limit to the search, which allows the use of quickly converging search methods to find the RSW velocity. Furthermore, by comparing the RSW velocity with the limit velocity, conditions under which pseudo-surface waves exist and dominate the response of the material can be determined. The method was tested on many different crystal symmetries and directions of propagation, and the advantages and disadvantages are discussed. An alternative method of finding the RSW velocity is then discussed that is based on finding the surface impedance matrix. This method is slower but is much more robust in actually converging to the RSW velocity when local minima are obscuring the answer in the boundary condition determinant.

2. Elastic wave propagation at the boundary

For the sake of consistent notation, the fundamentals of wave propagation in elastic media will be given here. The goal of the analysis is to determine the surface wave velocity in an elastic media given a certain propagation direction along a surface cut along an arbitrary crystallographic plane. Thus, a form of a solution that would indicate surface wave propagation at an unknown velocity is substituted in to the governing equations of elasticity and traction-free boundary conditions are then applied, and the velocity that satisfies the boundary conditions is considered a true surface wave velocity.

The governing equations of motion in a linear, anisotropic, homogeneous medium with no force terms are stated using summation notation as:

$$\rho \frac{\partial^2 u_i}{\partial t^2} = C_{ijkl} \frac{\partial^2 u_k}{\partial x_j x_l} \tag{1}$$

In this equation, ρ is the mass density, u_i is the displacement in the ith direction, and C_{ijkl} is the elastic stiffness tensor. The solution to this equation that would coincide with a wave propagating on the surface of the sample can be written as:

$$\mathbf{u} = \mathbf{a} e^{-\mathrm{ik}(\mathbf{m}\cdot\mathbf{x} + p\mathbf{n}\cdot\mathbf{x} - vt)} \tag{2}$$

Here, $\mathbf{a}$ is polarization vector that describes the particle displacements of the wave, $\mathrm{i} = \sqrt{-1}$, $\mathbf{m}$ is a unit vector in the direction of propagation of the wave, $\mathbf{n}$ is an outwardly pointed unit vector normal to the surface of the sample on which

the wave propagates and is orthogonal to $\mathbf{m}$, p is a complex constant to be determined, v is the velocity of the wave, and k is the wave number. Note that any point inside the half-space results in $\mathbf{n}\cdot\mathbf{x}$ being negative. This equation is simply a statement that there is a wave with velocity v traveling in the $\mathbf{m}$ direction on the surface of a half-space that has the outward normal vector $\mathbf{n}$. Since $\mathbf{m}$ is specified as a real unit vector, it travels infinitely in the $\mathbf{m}$ direction with no decay. However, the addition of complex p in front of the $\mathbf{n}\cdot\mathbf{x}$ term indicates there is both an oscillating term as well as a decay term (assuming $\mathrm{Im}\{p\} < 0$) in this direction, which is crucial for a surface wave to exist. As stated earlier, the surface wave cannot propagate into the sample, thus it must decay with respect to the distance away from the surface. Furthermore, the thickness of this layer, and thus the value of the imaginary component of p, is dependent on the wave velocity. However, the wave velocity is unknown at this point, which means p and v must be determined simultaneously.

One way to solve this equation would be to plug (2) into (1). Using the procedure shown in [5], we can define the 3×3 matrices:

$$\begin{aligned}\mathbf{Q} &= \{Q_{i,k}\} = \left\{\sum_{i,j=1}^{3} C_{ijkl} - \rho v^2 \delta_{i,k}\right\}\\ \mathbf{R} &= \{R_{i,k}\} = \left\{\sum_{i,j=1}^{3} C_{ijkl} m_j n_l\right\}\\ \mathbf{T} &= \{T_{i,k}\} = \left\{\sum_{i,j=1}^{3} C_{ijkl} n_j n_l\right\}\end{aligned} \tag{3}$$

In these expressions, $\delta_{i,k}$ is a Kronecker delta and m_i and n_i is are the ith component of the $\mathbf{m}$ and $\mathbf{n}$ vectors, respectively. These can be used to simplify the resulting expression from plugging (2) into (1) down to:

$$\left[\mathbf{Q} + p\left(\mathbf{R} + \mathbf{R}^T\right) + p^2\mathbf{T}\right]\mathbf{a} = \mathbf{0} \tag{4}$$

where $\mathbf{a}$ is the vector of constants. This is the quadratic eigenvalue problem that results from satisfying the equations of elasticity for a plane wave, with p being the eigenvalue and $\mathbf{a}$ the eigenvector. At this point, if the wave velocity was known, it could be used to solve this eigenvalue problem numerically to calculate the a_i and p and thus know the wave profile entirely.

The Rayleigh wave velocity is still unknown at this point. A further step of satisfying the boundary conditions must be taken to calculate it. The traction at the surface $\mathbf{n}\cdot\mathbf{x} = 0$ is expressed as:

$$\mathbf{t} = -\mathrm{ik}\mathbf{b}\mathrm{e}^{-\mathrm{ik}(\mathbf{m}\cdot\mathbf{x} - vt)} \tag{5}$$

where the vector $\mathbf{b}$ is given by

$$\mathbf{b} = \left(\mathbf{R}^T + p\mathbf{T}\right)\mathbf{a} \tag{6}$$

Equations (4) and (6) can be combined to give the new 6×6 eigenvalue problem known as the Stroh eigenvalue problem:

$$\mathbf{N}\begin{bmatrix}\mathbf{a}\\ \mathbf{b}\end{bmatrix} = p\begin{bmatrix}\mathbf{a}\\ \mathbf{b}\end{bmatrix}, \tag{7}$$

where

$$\mathbf{N} = \begin{bmatrix}\mathbf{T}^{-1}\mathbf{R}^T & \mathbf{T}^{-1}\\ -\mathbf{Q} + \mathbf{R}\mathbf{T}^{-1}\mathbf{R}^T & -\mathbf{R}\mathbf{T}^{-1}\end{bmatrix}. \tag{8}$$

This is a linear eigenvalue problem for calculating the eigenvector $\mathbf{a}$ and the eigenvalue p. However, there are 6 eigenvalues and 6 eigenvectors that satisfy this equation. In the range of velocities between 0 and the limiting velocity (discussed in Section 3.1), the eigenvalues are all complex and come in conjugate pairs. If the 3 eigenvalues and eigenvectors satisfying $\mathrm{Im}\{p\} < 0$ are labeled with the index $\alpha = 1, 2, 3$, the traction at the surface (5) can then be written as a linear combination of the three eigenvalue/eigenvector pair solutions:

$$\mathbf{t} = -\mathrm{ike}^{-\mathrm{ik}(\mathbf{m}\cdot\mathbf{x} - vt)}\sum_{\alpha=1}^{3} c_\alpha \mathbf{b}_\alpha = \mathbf{0}$$

where c_α are arbitrary complex constants that are not all equal to zero. This can be rewritten as:

$$\begin{bmatrix}\mathbf{b}_1 & \mathbf{b}_2 & \mathbf{b}_3\end{bmatrix}\begin{bmatrix}c_1\\ c_2\\ c_3\end{bmatrix} = \mathbf{B}\mathbf{c} = \mathbf{0} \tag{9}$$

This implies that the boundary condition at the free surface is satisfied when the matrix of eigenvectors, **B** is singular, ultimately leading to the expression:

$$\det\{\mathbf{B}\} = 0 \tag{10}$$

The velocity that satisfies this condition satisfies both the governing equations as well as the boundary conditions, and thus constitutes a viable surface wave velocity. In a numerical scheme the velocity is iterated over until the condition (10) is satisfied. Algorithms of this type have been suggested since as early as [16], though even earlier references allude to computational frameworks to calculate the Rayleigh wave velocity numerically. However, with the surge of research in applying the mathematical rigor of the Stroh formalism to the calculation of Rayleigh wave velocities in the 2000's, new results are available that make the numerical algorithms much more stable and quick, which is absolutely critical for using them in the context of materials characterization.

Another important concept in the analysis of surface waves is the surface impedance matrix, defined as:

$$\mathbf{Z} = -\mathrm{i}\mathbf{B}\mathbf{A}^{-1} \tag{11}$$

where **A** is the matrix formed by combining the displacement vectors, **a** into a single matrix. The inverse is guaranteed to exist in the event that (4) has three distinct eigenvalue solutions and complex conjugate solutions. In the event that this equation results in repeated eigenvalues, generalized eigenvectors can be computed, and these vectors are used in forming the matrix **A**. In either case, the eigenvectors are independent, and thus the matrix inverse exists. The surface impedance matrix will be used when direct calculation of RSW velocities with (10) is not feasible. In the next sections, a numerical algorithm is detailed which is very stable for calculation of the entire curve for Rayleigh waves on the surface of an arbitrarily oriented single crystal.

3. Numerical scheme

Rayleigh surface wave velocities can be calculated by finding the zeros of equation (10) above. The algorithm starts at a certain velocity, assembles the sub-matrices (3), calculates the eigenvectors and eigenvalues from (7), selects the eigenvectors that predict a decaying solution (i.e. negative imaginary components in the eigenvalues) and assembles the matrix **B** and calculate its determinant. The velocity is then iteratively changed until the zero is found.

3.1. Limiting velocity calculation

There are some difficulties that arise when trying to take advantage of the modern computation routines for 1-D root finding. For instance, there is only a finite region where the eigenvalues of **N** are complex and come in conjugate pairs. Even building the **B** matrix outside of this range is not straight forward for a computational routine. The typical solution to this problem is that found in Farnell [4], where the real eigenvalue that gives the lowest absolute value of the determinant of **B** is used. This can lead to discontinuities in the determinant function which precludes the use of gradient based optimization algorithms. Furthermore, it induces multiple local minima that have to be sorted through after the optimization has been performed. However, in any crystal system in which the stiffness matrix is defined to be positive definite (a condition that should be true in almost all cases), the eigenvalues are guaranteed to be complex and in conjugate pairs at $v = 0$ (see Lemma 1.1 in [5]). Furthermore, there is a velocity, $v_l > 0$, after which two or more of the eigenvalues become real. Finding this velocity before starting the iterative procedure greatly enhances the stability of modern computational routines for finding the roots of a function. Thus, to begin the algorithm in an arbitrary crystallographic direction, the limiting velocity is found first.

In [5], a method of finding the limiting velocity analytically for certain crystallographic orientations was given. This method is also convenient to implement numerically so that the limiting velocity can be found in any arbitrary direction in any crystallographic plane of an arbitrary crystal. The method starts by defining an angle, ϕ, used to define rotated unit vectors:

$$\begin{aligned} \tilde{m}_i(\phi) &= m_i\cos(\phi) + n_i\sin(\phi) \\ \tilde{n}_i(\phi) &= m_i\sin(\phi) + n_i\cos(\phi) \end{aligned} \tag{12}$$

The vectors $\tilde{\mathbf{m}}$ and $\tilde{\mathbf{n}}$ are the **m** and **n** vectors, rotated by an angle ϕ about the vector perpendicular to both of them, or $\mathbf{m}\times\mathbf{n}$. This basically rotates the plane and direction of propagation about the vector pointing out of the paper. A rotated **Q** matrix is then given as:

$$\tilde{Q}_{ik}(\phi) = (c_{ijkl} - \rho v^2 m_j m_l \delta_{ik})\tilde{m}_j\tilde{m}_l \tag{13}$$

This can be expanded by substituting (12) and written as:

$$\tilde{Q}_{ik}(\phi) = c_{ijkl}\left(m_j m_l\cos^2(\phi) + (m_j n_l + m_l n_j)\cos(\phi)\sin(\phi) + n_j n_l\sin^2(\phi)\right) - \rho v^2\delta_{ik}\cos^2(\phi) \tag{14}$$

Simplifications were made in this expression by recognizing that $m_i n_i = \mathbf{m} \cdot \mathbf{n} = 0$ and that $m_i m_i = n_i n_i = 1$. This expression can then be written in equation form by using (3). This is written as:

$$\begin{aligned} \tilde{\mathbf{Q}}(\phi) &= \mathbf{D}(\phi) - \rho v^2 \cos^2(\phi) \mathbf{I}_{3\times 3} \\ \mathbf{D}(\phi) &= \mathbf{Q}\cos^2(\phi) + \left(\mathbf{R} + \mathbf{R}^T\right)\cos(\phi)\sin(\phi) + \mathbf{T}\sin^2(\phi) \end{aligned} \tag{15}$$

The matrix $\mathbf{D}(\phi)$ is known as the acoustical tensor. It is shown in Lemma 1.1 of [5] that this matrix is positive definite for all ϕ, and thus has 3 real, positive eigenvalues. It can be seen from (15) that the eigenvalues of the matrix $\tilde{\mathbf{Q}}$ are then expressed as:

$$g_i(\phi) = \lambda_i(\phi) - \rho v^2 \cos^2(\phi) \tag{16}$$

where $\lambda_i(\phi)$ is the ith eigenvalue of $\mathbf{D}(\phi)$. Lastly, the definition of the limiting velocity is the smallest velocity for which the matrix $\tilde{\mathbf{Q}}(\phi)$ becomes singular for some angle, ϕ. Furthermore, $\tilde{\mathbf{Q}}(\phi)$ is positive definite at velocities below the limiting velocity but greater than or equal to zero. Thus, the smallest velocity for which $\tilde{\mathbf{Q}}(\phi)$ becomes singular is the point at which the smallest eigenvalue of $\tilde{\mathbf{Q}}(\phi)$ is zero. This problem can be written as:

$$v_L = \min_{\phi \in \{-90,90\}} \sqrt{\frac{\lambda_1(\phi)}{\rho}} \frac{1}{|\cos(\phi)|} \tag{17}$$

This is a bounded 1D optimization that requires only one 3×3 eigenvalue solution per evaluation point. This problem can be solved by using a standard golden section search or any other found in e.g. [17]. On a laptop PC this computation takes roughly 1.7 ms, which for comparison is less than an order of magnitude higher than the computation time required for one addition in Matlab.

3.2. RSW velocity calculation

Once the limiting velocity is known, one method of finding the Rayleigh wave velocity is to iterate over v until a root of the determinant is found. This works well in certain crystal systems where the determinant is well behaved, such as in cubic crystal systems. For instance, consider a nickel alloy material where the stiffness matrix is given by:

$$\mathbf{C} = \begin{bmatrix} 2.41 & 1.47 & 1.47 & 0 & 0 & 0 \\ 1.47 & 2.41 & 1.47 & 0 & 0 & 0 \\ 1.47 & 1.47 & 2.41 & 0 & 0 & 0 \\ 0 & 0 & 0 & 1.26 & 0 & 0 \\ 0 & 0 & 0 & 0 & 1.26 & 0 \\ 0 & 0 & 0 & 0 & 0 & 1.26 \end{bmatrix} \times 10^{11} \text{ Pa}. \tag{18}$$

The density is assumed to be $\rho = 8910$ kg/m^3. We seek the RSW velocity for a wave traveling in the x_1-direction along the crystallographic plane given by the Euler angles [15 45 8] in Bunge's active notation. This corresponds to:

$$\begin{aligned} \mathbf{m} &= \{0.9311 \quad 0.3514 \quad 0.0984\}^T \\ \mathbf{n} &= \{0.1830 \quad -0.6830 \quad 0.7071\}^T \end{aligned} \tag{19}$$

The RSW velocity will be the velocity for which $|\mathbf{B}| \times |\mathbf{B}|^* = 0$. Plotting this quantity with respect to the velocity gives the curve shown in Fig. 1. This curve was plotted from 0 velocity to the limiting velocity in this direction. The RSW velocity is the point at which the function value is zero, which is also the global minimum of the curve in the interval given due to taking the norm squared of the determinant value. This minimum can be found by using golden section search.

This method works well for cubic crystal systems because the determinant equations typically result in curves that look similar to Fig. 1. However, there are pathological examples that make this algorithm unstable for certain directions in some crystal systems. For instance, consider the hexagonal Zinc system with stiffness matrix:

$$\mathbf{C} = \begin{bmatrix} 1.68 & 0.782 & 0.710 & 0 & 0 & 0 \\ 0.782 & 1.68 & 0.710 & 0 & 0 & 0 \\ 0.710 & 0.710 & 1.89 & 0 & 0 & 0 \\ 0 & 0 & 0 & 0.546 & 0 & 0 \\ 0 & 0 & 0 & 0 & 0.546 & 0 \\ 0 & 0 & 0 & 0 & 0 & 0.449 \end{bmatrix} \times 10^{11} \text{ Pa}. \tag{20}$$

and density $\rho = 7180$ kg/m^3. This system gives the algorithm troubles when trying to compute RSW velocity in all directions on the (010) plane, which corresponds to Euler angles [0 90 0]. An example curve can be seen in Fig. 2. There are several

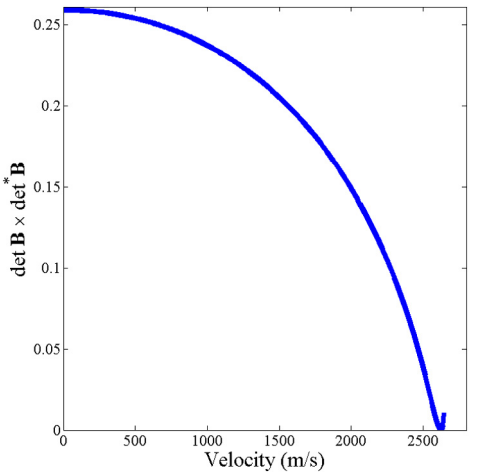

Fig. 1. A plot of the determinant of **B** times the conjugate of the determinant of **B** with respect to the velocity in a cubic crystal.

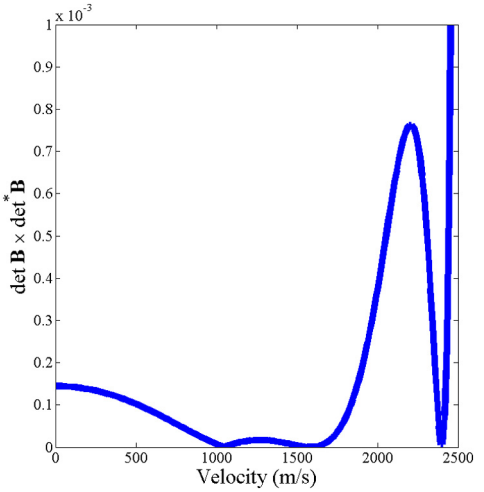

Fig. 2. A plot of the determinant of **B** times the conjugate of the determinant of **B** with respect to the velocity in a hexagonal crystal.

different minima in this curve which seek to confuse the algorithm. The last minimum is the value that corresponds to the RSW velocity in this material. The curve could be sampled many times to find all the minimum values, but this leads to computational inefficiencies that are exacerbated when used within an inversion algorithm. Thus, it is desirable to find a new method for locating this minima.

In [18], a result is given that is capable of locating the RSW velocity without relying on the boundary value determinant. In this paper, it is noted that the surface impedance matrix, **Z**, is positive definite for $0 \leq v < v_R$. This implies that the eigenvalues of **Z** are all positive until the velocity reaches v_R, at which point one of the eigenvalues becomes zero. Furthermore, as observed in [19], there is only one zero eigenvalue at the Rayleigh wave velocity, and the eigenvalues are monotonically decreasing as a function of v in the range $0 \leq v < v_L$. Thus, if the eigenvalues are sorted in ascending order, the first eigenvalue will have a sign change at $v = v_R$. Again, this leads to a quick and accurate method for obtaining the velocity when the limiting velocity is already known. The drawback to this is that it takes longer to compute the eigenvalues of Z than simply using the **b** vectors to compute the determinant of **B**. In fact, using the standard algorithms in Matlab's fminbnd function, the RSW velocity takes ∼7 ms to compute by using the boundary value determinant, whereas using the fzero algorithm on the smallest eigenvalue of Z takes ∼20 ms. Still, this leads to one forward simulation of 180 degrees of orientation taking ∼3.6 seconds, which is feasible for use in an inversion algorithm.

4. Alternate modes

In many crystals, more than one surface wave mode may exist. This computational routine is intended to solve for elastic constants given observed surface wave speeds in multiple directions on a single crystal. Thus it is important to be able to

predict velocities of waves that are not fundamentally Rayleigh-like in nature. Two such waves will be discussed in this section corresponding to the crystals shown above.

4.1. Pseudo-surface waves in cubic materials

It has been long known that in certain directions on certain surfaces of cubic crystals, pseudo-surface waves will propagate that will dominate the response over RSW's [20]. A pseudo-surface wave is one which propagates on the surface for a short distance. Portions of the energy propagate into the sample, leading to decay in the propagation direction. Mathematically, this can be expressed as:

$$\mathbf{u} = \mathbf{a}\mathrm{e}^{-\mathrm{ik}(q\mathbf{m}\cdot\mathbf{x}+p\mathbf{n}\cdot\mathbf{x}-vt)} \tag{21}$$

where $q = 1 + b\mathrm{i}$ is a complex constant that indicates decay in the propagation direction. The decay term, $b \leq 0$, is now a new constant that needs to be estimated alongside the surface wave velocity. Carrying this term through the derivations of Stroh's eigenvalue problem gives a new $\mathbf{N}$ matrix given by

$$\mathbf{N}' = \begin{bmatrix} q\mathbf{T}^{-1}\mathbf{R}^T & \mathbf{T}^{-1} \\ -\mathbf{Q}' + q^2\mathbf{R}\mathbf{T}^{-1}\mathbf{R}^T & -q\mathbf{R}\mathbf{T}^{-1} \end{bmatrix}, \tag{22}$$

where

$$\mathbf{Q}' = \{Q'_{i,k}\} = \left\{ \sum_{i,j=1}^{3} q^2 C_{ijkl} - \rho v^2 \delta_{i,k} \right\}. \tag{23}$$

The eigenvalues and eigenvectors of $\mathbf{N}'$ are used in the same way to predict the zeros of the boundary value determinant. However, with the addition of the complex terms in the matrix, the eigenvalues no longer appear in complex conjugate pairs. Furthermore, the third eigenvalue will actually have $\mathrm{Im}\{p\} > 0$, which would indicate that energy increases as depth approaches infinity. This increase is offset by the decay in the direction of propagation.

When the algorithm encounters a condition where the RSW velocity is near the limiting velocity:

$$v_R \geq 0.99 v_L \tag{24}$$

it searches for supersonic solutions to the boundary value problem that are just above the limiting velocity. The boundaries of the optimization are moved to ($v_L < v <= v_N$), and optimization performed again. In the current iteration of the algorithm, v_N is chosen to be the point at which there are more than 2 real eigenvalues, which can be found by an iterative search routine.

The solutions to this new optimization problem may not be zeros, but they are minima of the boundary value determinant. If they are not zeros, the decay term is added to the eigenvalue problem and the search is continued on both b and v. The advantage to this approach is that this second optimization is performed only in the directions at which a pseudo-surface wave is likely to exist. As the algorithm progresses through more directions, the previously calculated pseudo-surface wave velocity can be used as an initial guess to make the second optimization converge very quickly.

4.2. Alternate surface wave modes in non-cubic materials

Surface waves propagating on the basal plane of hexagonal crystals do not behave like typical Rayleigh waves. The dominant surface wave mode on this specific crystallographic plane is a supersonic, 2-component wave (according to the classification system from [21]). The velocity of this wave was predicted analytically by [22]. As the cut-plane tilts away from the basal plane, this supersonic mode eventually gives way to the traditional subsonic RSW with all three components. In the configuration in which the free surface normal lies in the Basal plane, the surface waves that propagate in any direction are purely traditional Rayleigh waves and their velocities have been predicted in certain directions by many authors (e.g. [23]). The condition for the existence of this alternate propagation mode in hexagonal crystals is the same as that for the PSW in cubic crystals, and the method of finding the velocity is also the same. The calculations were verified on a hexagonal crystal analyzed previously in [24]. In that work, the authors performed computations for a number of different crystals with the reference plane of the surface wave coincident with a plane of symmetry of a the crystal system. Their plots show propagation of surface waves along a surface with the angle between the surface normal and the main axis, or c-axis, of the hexagonal material varying between 0 and 90 degrees. The algorithms from the current work were used to calculate this curve for cadmium telluride, and the data is shown in Fig. 3. This plot shows the same surface wave velocity as "Fig. 11" from [24].

To test this algorithm on more complex material systems, a monoclinic material was analyzed as well. In [25], the authors discussed propagation of surface waves when the plane of symmetry in monoclinic materials was spanned by the normal to the free surface as well as the direction of propagation, $\mathbf{n}$ and $\mathbf{m}$, in the notation used in this paper. They gave an in-depth analysis of the theory of wave propagation in this special case and showed a number of numerical examples.

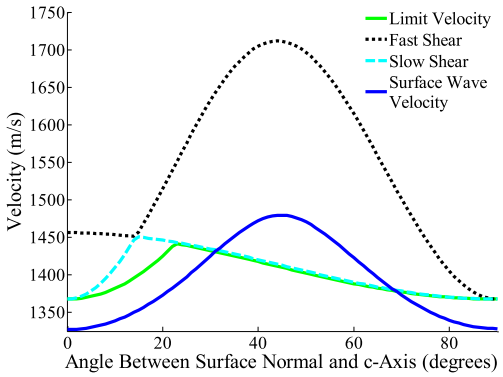

Fig. 3. Plot of the surface wave velocity, the limiting velocity, and the fast and slow shear wave velocities for cadmium telluride with the c-axis of the hexagonal crystal in the plane spanned by **m** and **n**. The x-axis is the angle of the primary axis of the hexagonal crystal with respect to the normal of the surface.

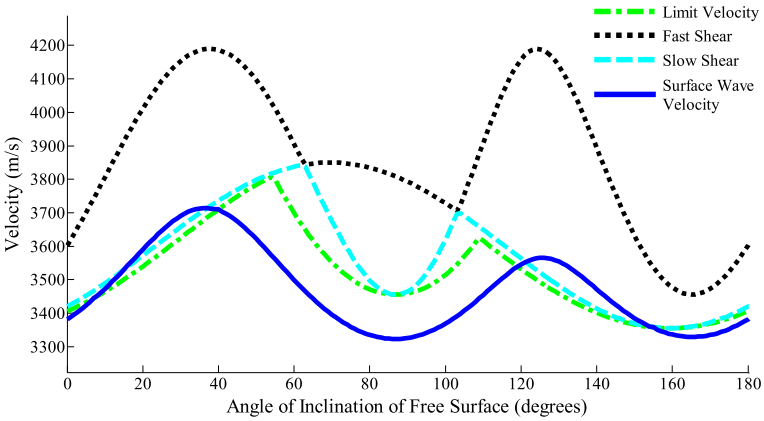

Fig. 4. Plot of the surface wave velocity, the limiting velocity, and the fast and slow shear wave velocities for aegirite–augite with the surface waves propagating in the plane of symmetry.

For the purpose of this work, one crystal that they analyzed, aegirite–augite, was used to calculate the surface wave velocity and compare with the results shown in this previous work. The curves shown in that work were calculated by keeping **n** and **m** in the plane of symmetry and rotating them by an angle, α, about the vector normal to them, essentially changing the angle of inclination of the stress free boundary relative to the crystal system. The results of the computation are shown in Fig. 4. Once again, the predicted surface wave velocity is the exact same curve as that shown in the paper by Chadwick and Wilson.

5. Verification of the numerical scheme

The algorithms for calculating surface wave velocities discussed in the previous section were verified using other numerical methods. This section shows these results as well as verification in the context of inverse algorithms for calculation of the elastic constants.

5.1. Calculation of surface wave velocity on certain cut-planes

A large set of experimental data sets on multiple different cut planes in a cubic nickel crystal was given in [2]. In this paper, two specific planes from [2] were picked to determine the agreement with experimental data. In their paper, Li et al. gave the crystallographic planes as Miller indices, so the indices were converted to Euler angles for use in the code. The same material properties as those found in the paper were used to generate the curves ($c_{11} = 235$ GPa, $c_{12} = 142$ GPa, $c_{11} = 131$ GPa, and $\rho = 8720$ kg/m^3). The velocities generated by the code discussed previously are given in Fig. 5. The first plot, Fig. 5a shows the velocities on the plane (0.28 0.1 1) and the second is for the plane (0 0.25 1). While the tilt in plane is different, the calculated velocities are the same as those shown in the paper, which also matched the experiments that were performed in that work. These figures take an average of $\sim$3 s to generate on a laptop computer with an Intel Core™i7-3630QM processor and 16 GB of DDR3 RAM.

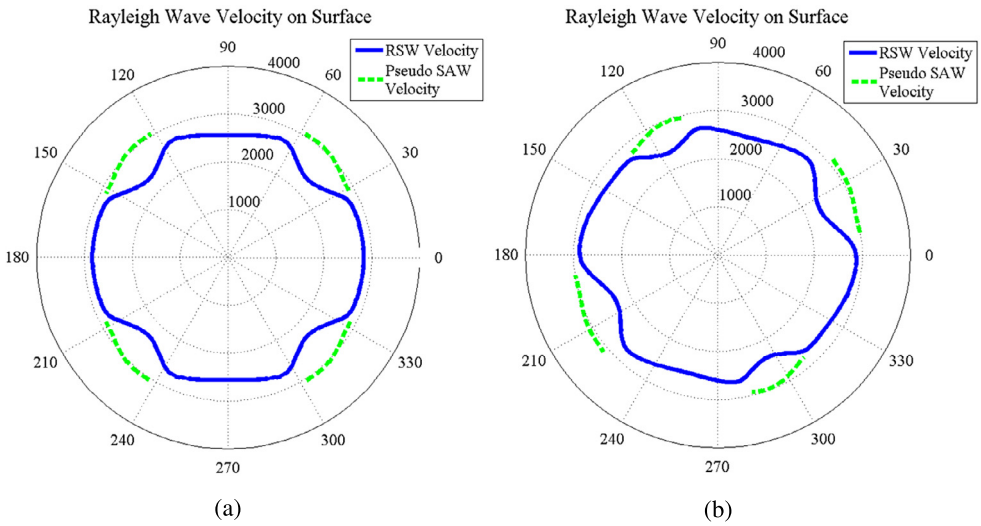

Fig. 5. Polar plots showing the RSW velocity and the PSW velocity on the nickel crystal used in [2]. (a) Shows the velocity on the (0 0.25 1) plane and (b) shows the velocity on the (0.28 0.1 1) plane.

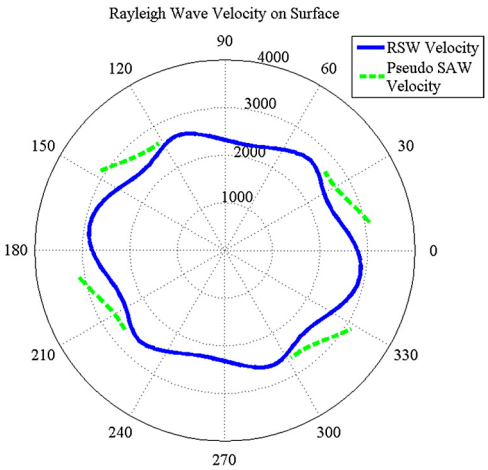

Fig. 6. Plot of the wave velocities on the plane used in the inverse problem verification.

5.2. Verification of the inverse problem on cubic materials

The inverse problem was tested with simulated data to verify convergence and test the sensitivity to the initial guess of the elastic constants. Velocity curves were generated using the elastic constants given in §3.2 on the cubic crystal given there for the plane described by the Euler angles [15 45 8]. Noise was added to the data and the inverse problem was run for multiple initial guesses of elastic constants to determine the convergence of the algorithm with increasingly poor starting points. The velocity profile at this orientation is shown in Fig. 6.

In an experiment, the velocity of sound is typically not measured directly. Instead, often the arrival time of a wave is measured at one point on a sample surface and then again on a different point separated by a distance, Δd. Thus, the noise in the experiment will likely be on the measured arrival time. In lieu of this, synthetic data was generated by adding independent and identically distributed (IID) noise to the calculated change in arrival time for the waves in each direction:

$$t_i^{synth} = t_i^{calc} + \varepsilon_i = \frac{\Delta d}{v_i^{calc}} + \varepsilon_i$$
$$\varepsilon_i \sim Normal(0, \sigma^2) \tag{25}$$

The calculated arrival time, t_i^{calc}, is determined by calculating the velocity in the ith direction, v_i^{calc} and dividing an assumed spacing between measurement points by this velocity. The assumption that the noise in the data is IID and normal is

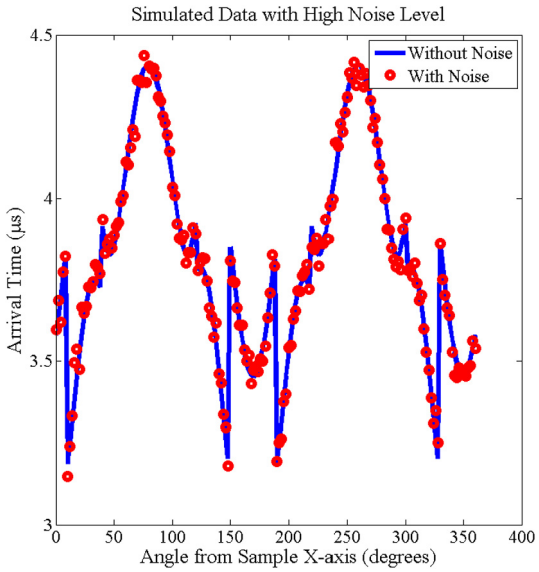

Fig. 7. The arrival times as a function of angle away from the sample X axis, with the solid line showing the computed arrival times and the scatter plot showing the arrival times with noise added.

assumed to be valid in the experiment, though possible deviations should be addressed if the assumptions do not appear valid from analysis of the data. This allows the algorithm to take advantage of the typical nonlinear least squares estimates:

$$\begin{aligned} &\underset{c_{ij}}{\text{argmin}} \quad \sum_{m=1}^{n}\left(t_m^{synth} - \frac{\Delta d}{v_m(c_{ij})}\right)^2 \\ &\text{subject to } c_{ij}^{lower} \le c_{ij} \le c_{ij}^{upper} \end{aligned} \tag{26}$$

The change in arrival time for the plane used in this section at a separation distance of .01 m is given in Fig. 7. The simulated data is plotted on top of the calculated arrival times. In this study, a standard deviation of 3×10^{-8} s was used to generate the noise in the data. This number was chosen based on previous experience with peak fitting for finding the time of arrival of Rayleigh surface waves. The experimental setup in the lab was discussed in [26]. Though no number was given there for the standard deviation of time of arrival, 3×10^{-8} s has been typical for this experiment.

Two aspects of the forward problem make the inverse problem more challenging. Scaling is important factor in any optimization problem. For instance, the results of the simulation are in seconds, but the time of flight of waves in an ultrasound experiment are generally on the order of μs. Therefore, the objective function shown in (26) is multiplied by a factor of 1e6. Furthermore, elastic constants are generally on the order of 1e11, so the parameters of the inverse function are divided by this factor. This ensures that the scales of the objective function and parameters are similar. Another confounding factor is that the gradients of the problem are not currently calculated analytically. Furthermore, the objective function is itself a minimization problem which is subject to non-negligible noise due to the convergence criteria of the inner optimization problem. Finite difference methods for gradient computation tend to enhance the strength of this noise to the point that derivative calculation with finite difference is very unreliable. A combination of finite difference for the eigenvalue problem and analytical derivatives for the optimization/root finding algorithm can be used to reliably compute the sensitivities, but this is at considerable computational cost. Thus, for this work, a non-gradient based Nelder–Mead optimization algorithm was used to perform the optimization in the inverse problem.

Another important observation is that the inverse problem is generally more well behaved for cubic crystals when the parameter estimates are performed on the alternative but equivalent parameterization:

$$\begin{aligned} E &= \frac{(c_{11}+2c_{12})(c_{11}-c_{12})}{c_{11}+c_{12}} \\ \nu &= \frac{c_{12}}{c_{11}+c_{12}} \\ \alpha &= \frac{2c_{44}}{c_{11}-c_{12}} \end{aligned} \tag{27}$$

This parameterization is essentially the Young's modulus, Poisson ratio, and the Zener anisotropy ratio of the material, respectively. The sensitivity of the velocity with respect to these two parameterizations were computed at the known elastic constants and are plotted in Fig. 8. It can be seen in these plots that the sensitivity to c_{11} and c_{12} are both very similar

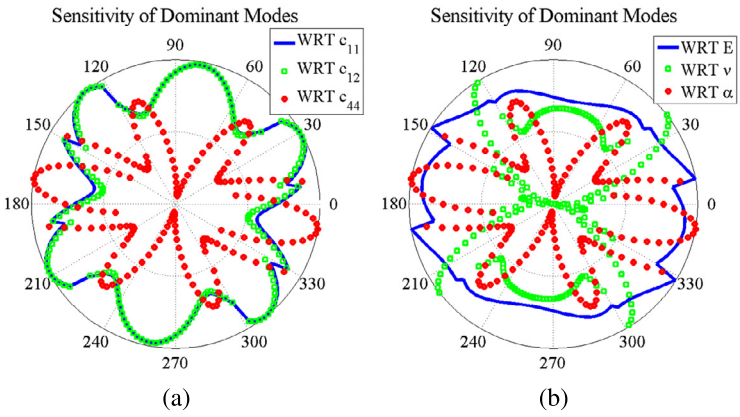

Fig. 8. Figures showing the sensitivity of the dominant wave mode velocity with respect to (a) the c_{ij} parameterization and (b) the E, ν, and α parameterization.

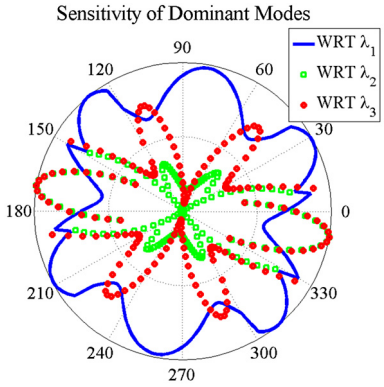

Fig. 9. The sensitivity of the dominant wave mode velocity with respect to the eigenvalue parameterization.

for all the directions of propagation, which would tend to indicate identifiability issues with these two parameters. This is not an issue with the E, ν, and α parameterization. An alternative parameterization could be to use the eigenvalues of the stiffness matrix as the parameters for the inverse problem, or:

$$\begin{aligned}\lambda_1 &= c_{11} - c_{12}\\ \lambda_2 &= c_{11} + 2c_{12}\\ \lambda_3 &= 2c_{44}\end{aligned} \tag{28}$$

This parameterization has the added advantage of simply being able to place bounded constraints on the optimization to keep the eigenvalues positive, thus enforcing positive definite stiffness matrices. However, the sensitivities (shown in Fig. 9) have similar issues as those from the usual c_{ij} parameterization between λ_2 and λ_3. Thus, the E, ν, and α parameterization is used in the inverse problem, and the results of the inverse are converted back to the usual c_{ij} after an optimal solution has been found.

The inverse problem was run with multiple different initial design points. The known values of the elastic constants that generated the data were $[2.41, 1.47, 1.26] \times 10^{11}$ Pa. Initial design points were selected randomly by assuming a uniform distribution in a reasonable range of E, ν and α. The table of the initial design points is shown in Table 1. The final values for each starting point are shown in Table 2. It is clear that the initial designs all underestimated the values of c_{ij}, the most egregious of which are points 4–7. However, the only design points that did not converge to the correct minimum are points 2, 3, and 8. These points had initial values that were relatively close to the true values, with 3 being the closest out of all the initial designs. This strange behavior is likely due to the algorithm used for the optimization not being able to effectively linearize the problem around these design points. This is because of the numerical error in the inner optimization loop from Equation (10). However, the values of the objective function are three orders of magnitude lower for points 1, 4–7, and 9–10 than they are for the troubled values, and it is clear that the algorithm can actually be used effectively in the inverse problem provided multiple initial designs are sampled. Strides should be taken to improve the gradient estimation so that a gradient-based approach for the inverse problem can be used rather than the linearized simplex algorithms.

Table 1
Starting points attempted for inverse (1e11 Pa).

Point number	c_{11}	c_{12}	c_{44}
1	1.9201	1.0669	0.9903
2	2.0366	0.9923	1.1760
3	2.3138	1.3255	1.1245
4	1.5680	0.7683	1.0896
5	1.5746	0.7735	1.0384
6	1.5329	0.7445	0.9812
7	1.4871	0.7323	0.8413
8	1.8068	0.8971	1.0227
9	1.9947	0.9992	1.0723
10	2.1144	1.1001	1.3895

Table 2
Final values for each starting point (1e11 Pa).

Point number	c_{11}	c_{12}	c_{44}
1	2.3365	1.3942	1.2683
2	4.2637	3.3114	1.1234
3	4.1307	3.1769	1.1174
4	2.3365	1.3941	1.2683
5	2.3364	1.3940	1.2683
6	2.3399	1.3976	1.2681
7	2.3365	1.3941	1.2683
8	4.8179	3.8537	1.0951
9	2.3364	1.3940	1.2683
10	2.3365	1.3941	1.2683

6. Summary

A new numerical scheme was developed for calculating the velocity of the dominant surface wave mode in anisotropic elastic media. The algorithm was applied to hexagonal and cubic crystals and found to be accurate. The method takes 3 seconds to build an entire velocity curve for 181 angles of wave propagation on an arbitrary face of a crystal, which is a significant improvement in the amount of time previous implementations of numerical schemes have taken. The algorithm was applied in the numerical inverse problem for calculating the elastic constants of a cubic crystal with data generated by adding IID noise to the time-of-arrivals. The algorithm converged to the correct minimum in the inverse problem for seven out of 10 initial designs, and improvements in the gradient computation could result in the use of gradient-based optimization algorithms which do not have as much sensitivity to the initial design point. This remains as future work.

Acknowledgements

S. Sathish would like to acknowledge support from the Materials & Manufacturing Directorate of the Air Force Research Laboratory through contract number: FA8650-14-D-5224. The authors would also like to acknowledge Dr. Amanda Criner for the valuable support and discussions on this work.

References

[1] M. Mendik, S. Sathish, A. Kulik, G. Gremaud, P. Wachter, Surface acoustic wave studies on single-crystal nickel using Brillouin scattering and scanning acoustic microscope, J. Appl. Phys. 71 (6) (1992) 2830–2834.
[2] W. Li, S.D. Sharples, R.J. Smith, M. Clark, M.G. Somekh, Determination of crystallographic orientation of large grain metals with surface acoustic waves, J. Acoust. Soc. Am. 132 (2) (2012) 738–745.
[3] D. Gasteau, N. Chigarev, L. Ducousso-Ganjehi, V. Gusev, F. Jenson, P. Calmon, V. Tournat, Single crystal elastic constants evaluated with surface acoustic waves generated and detected by lasers within polycrystalline steel samples, J. Appl. Phys. 119 (4) (2016) 043103.
[4] G. Farnell, Properties of elastic surface waves, Physical Acoustics 6 (1970) 109–166.
[5] K. Tanuma, Stroh formalism and Rayleigh waves, J. Elast. 89 (1–3) (2007) 5–154.
[6] T. Ting, Explicit secular equations for surface waves in an anisotropic elastic half-space from Rayleigh to today, in: Surface Waves in Anisotropic and Laminated Bodies and Defects Detection, Springer, 2004, pp. 95–116.
[7] A. Mielke, Y.B. Fu, Uniqueness of the surface-wave speed: a proof that is independent of the Stroh formalism, Math. Mech. Solids 9 (1) (2004) 5–15.
[8] M. Destrade, The explicit secular equation for surface acoustic waves in monoclinic elastic crystals, J. Acoust. Soc. Am. 109 (4) (2001) 1398–1402.
[9] T. Ting, An explicit secular equation for surface waves in an elastic material of general anisotropy, Q. J. Mech. Appl. Math. 55 (2) (2002) 297–311.
[10] D. Taylor, Surface waves in anisotropic media: the secular equation and its numerical solution, in: Proceedings of the Royal Society of London A: Mathematical, Physical and Engineering Sciences, vol. 376, The Royal Society, 1981, pp. 265–300.
[11] M. Cherry, S. Sathish, A. Pilchak, D.E. Chimenti, L.J. Bond, A synthetic aperture routine to approximate Rayleigh surface wave imaging scans over anisotropic media, in: AIP Conf. Proc., vol. 1650, AIP, 2015, pp. 1688–1696.
[12] L. Shi, Y. Zhou, J.-M. Wang, M. Zhuang, N. Liu, Q.H. Liu, Spectral element method for elastic and acoustic waves in frequency domain, J. Comput. Phys. 327 (2016) 19–38.

[13] X. Chen, C. Birk, C. Song, Transient analysis of wave propagation in layered soil by using the scaled boundary finite element method, Comput. Geotech. 63 (2015) 1–12.
[14] K. Gao, S. Fu, R.L. Gibson, E.T. Chung, Y. Efendiev, Generalized multiscale finite-element method (GMsFEM) for elastic wave propagation in heterogeneous, anisotropic media, J. Comput. Phys. 295 (2015) 161–188.
[15] P. Packo, T. Bielak, A. Spencer, T. Uhl, W. Staszewski, K. Worden, T. Barszcz, P. Russek, K. Wiatr, Numerical simulations of elastic wave propagation using graphical processing units—comparative study of high-performance computing capabilities, Comput. Methods Appl. Mech. Eng. 290 (2015) 98–126.
[16] T.C. Lim, G. Farnell, Search for forbidden directions of elastic surface-wave propagation in anisotropic crystals, J. Appl. Phys. 39 (9) (1968) 4319–4325.
[17] W.H. Press, The Art of Scientific Computing, 3rd Edition, Numerical Recipes, Cambridge University Press, 2007.
[18] D. Barnett, J. Lothe, Free surface (Rayleigh) waves in anisotropic elastic half-spaces: the surface impedance method, in: Proceedings of the Royal Society of London A: Mathematical, Physical and Engineering Sciences, vol. 402, The Royal Society, 1985, pp. 135–152.
[19] Y.B. Fu, A. Mielke, A new identity for the surface–impedance matrix and its application to the determination of surface-wave speeds, in: Proceedings of the Royal Society of London A: Mathematical, Physical and Engineering Sciences, vol. 458, The Royal Society, 2002, pp. 2523–2543.
[20] T. Lim, G. Farnell, Character of pseudo surface waves on anisotropic crystals, J. Acoust. Soc. Am. 45 (4) (1969) 845–851.
[21] T. Ting, D. Barnett, Classifications of surface waves in anisotropic elastic materials, Wave Motion 26 (3) (1997) 207–218.
[22] R. Stoneley, The seismological implications of aeolotropy in continental structure, Geophys. Suppl. Mon. Not. R. Astron. Soc. 5 (8) (1949) 343–353.
[23] D. Royer, E. Dieulesaint, Rayleigh wave velocity and displacement in orthorhombic, tetragonal, hexagonal, and cubic crystals, J. Acoust. Soc. Am. 76 (5) (1984) 1438–1444.
[24] P. Chadwick, Wave propagation in transversely isotropic elastic media. II. Surface waves, in: Proceedings of the Royal Society of London A: Mathematical, Physical and Engineering Sciences, vol. 422, The Royal Society, 1989, pp. 67–101.
[25] P. Chadwick, N. Wilson, The behaviour of elastic surface waves polarized in a plane of material symmetry II. Monoclinic media, Proceedings of the Royal Society of London A: Mathematical, Physical and Engineering Sciences, vol. 438, The Royal Society, 1992, pp. 207–223.
[26] S. Sathish, R.W. Martin, Quantitative imaging of Rayleigh wave velocity with a scanning acoustic microscope, IEEE Trans. Ultrason. Ferroelectr. Freq. Control 49 (5) (2002) 550–557.